Electronic Supplementary Material (ESI) for Organic & Biomolecular Chemistry.

Supplementary Information for

Chelated charge assisted halogen bonding enhanced halide recognition by a pyridinium-iodotriazolium axle containing [2]rotaxane

Alexander E. Hess and Paul D. Beer*

Synthesis – General Remarks

All commercial solvents and reagents were used as purchased, unless otherwise stated. Anhydrous solvents were degassed with N_2 and dried by passing them through an MBraun-800 column. Triethylamine was distilled and stored over KOH pellets. Tetrabutylammonium (TBA) salts and $Cu(MeCN)_4PF_6$ were stored in a vacuum desiccator with P_2O_5 desiccant. TBTA was prepared according to a literature procedure.[S1] Water was distilled and micro-filtered using a Milli-Q Millipore machine. Chromatography was undertaken using silica gel (particle size: 40-63 µm) or preparative TLC plates (20 x 20 cm, 1 cm silica thickness). Size exclusion chromatography was carried out using Biobeads SX-1 and $CHCl_3$ used as eluent.

^1H, ^{13}C and ^{19}F NMR spectra were recorded using Varian Mercury 300, Bruker AVIII400 and Bruker AVIII500 spectrometers. Mass spectra were recorded on a Waters LCT Premier instrument (low resolution MS) or a Bruker µTOF instrument (high resolution MS).

^{1}H NMR Titration Protocol

Titration experiments were performed on a Bruker AVIII500 spectrometer operating at 500 MHz for ^1H NMR and at a temperature of 298 K. An initial volume of 0.5 mL of host rotaxane at a concentration of 1.5 mM was used. Solutions of the respective anions (50 mM) as their TBA salts were added in aliquots, with spectra recorded at 0, 0.2, 0.4, 0.6, 0.8, 1.0, 1.2, 1.4, 1.6, 1.8, 2.0, 2.5, 3.0, 4.0, 5.0, 7.0, 10.0 equivalents added. Association constants were calculated form the data obtained using the software package WinEQNMR2[S2], following the internal pyridinium proton b. An estimate of the association constant and the observed chemical shifts of proton b from each spectrum recorded were added to the programs input file. Refinement of the data using a non-linear least-squares regression analysis gave an optimised fit between the observed and calculated data. Comparison of the experimental and calculated binding isotherms confirmed that a 1:1 binding model was appropriate with all anions studied.

Characterisation of axle precursors 3 – 6

Terphenyl-stoppered mono-methyl nicotinic ester 3

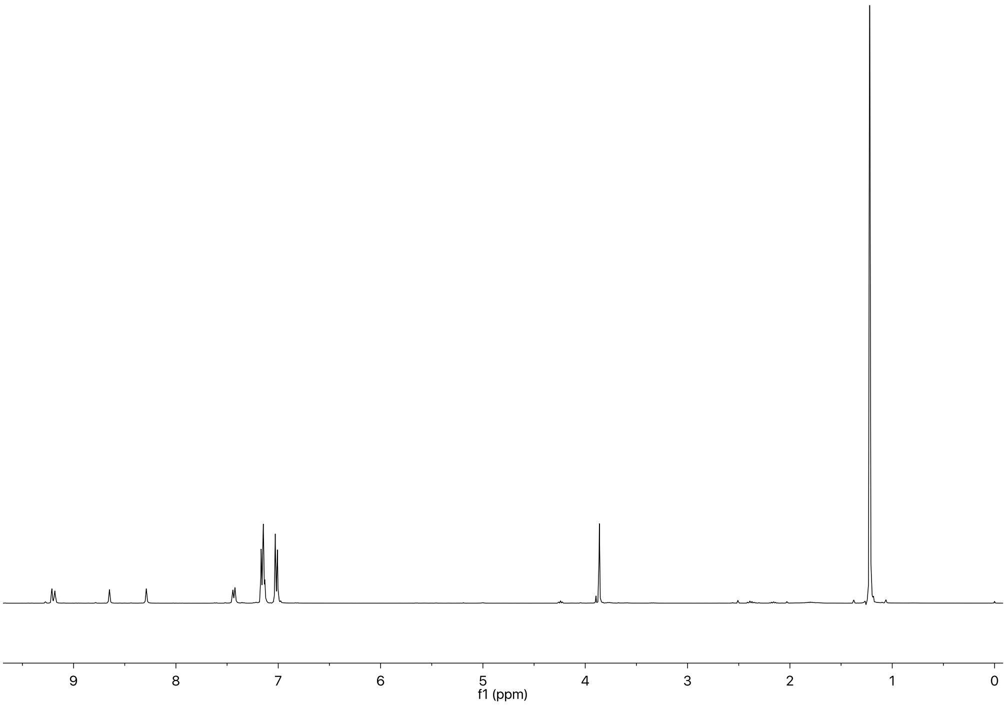

Figure S1 ^{1}H NMR spectrum of **3** ($CDCl_3$, 298 K, 400 MHz).

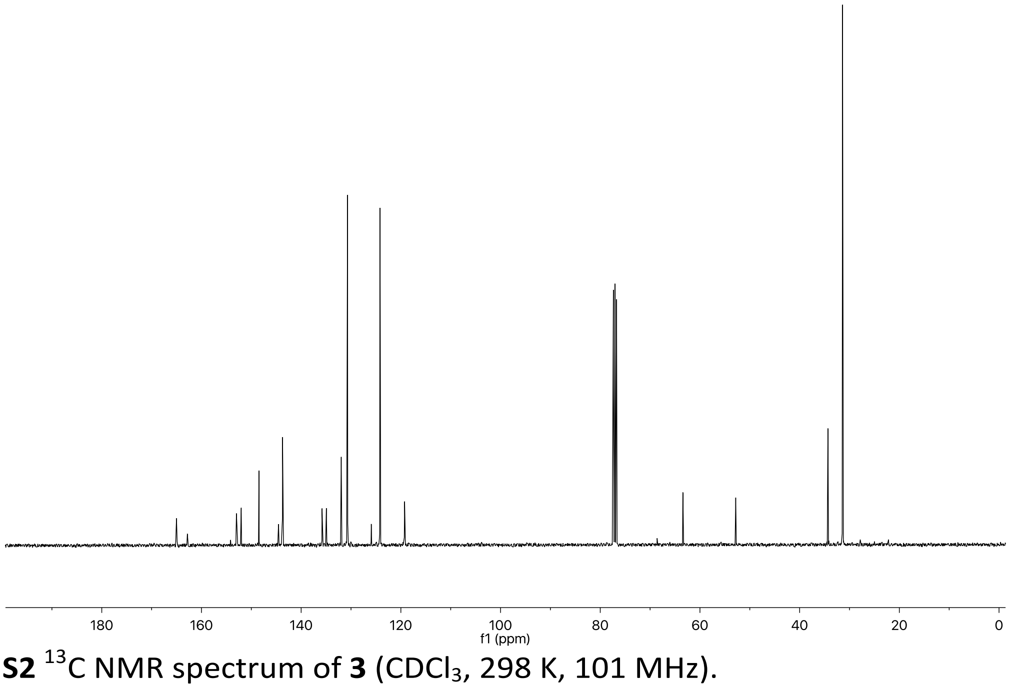

Figure S2 ^{13}C NMR spectrum of **3** ($CDCl_3$, 298 K, 101 MHz).

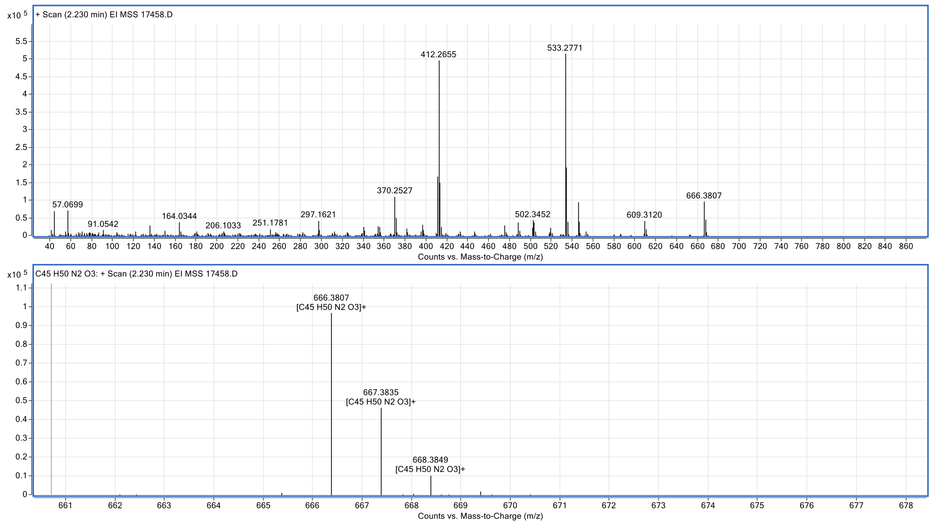

Best	Formula	Species	m/z	Diff (ppm)	Mass (MFG)
True	C45 H50 N2 O3	M+	666.3807	1.83	666.3821

Figure S3 GCMS-EI mass spectrum of **3**.

Terphenyl-stoppered nicotinic acid 4

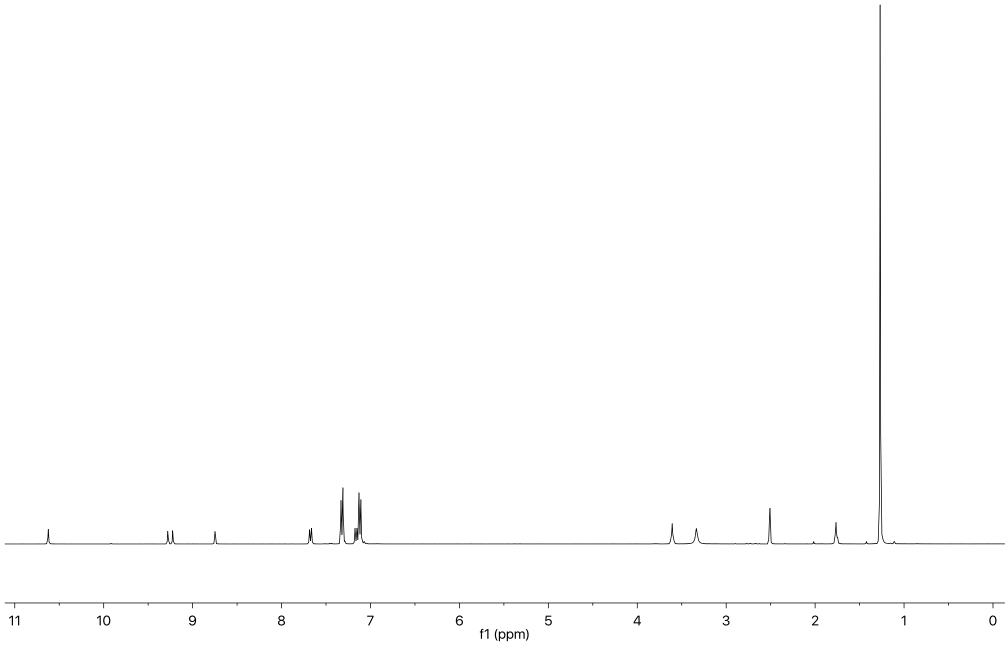

Figure S4 ^{1}H NMR spectrum of **4** (DMSO-d_6, 298 K, 400 MHz).

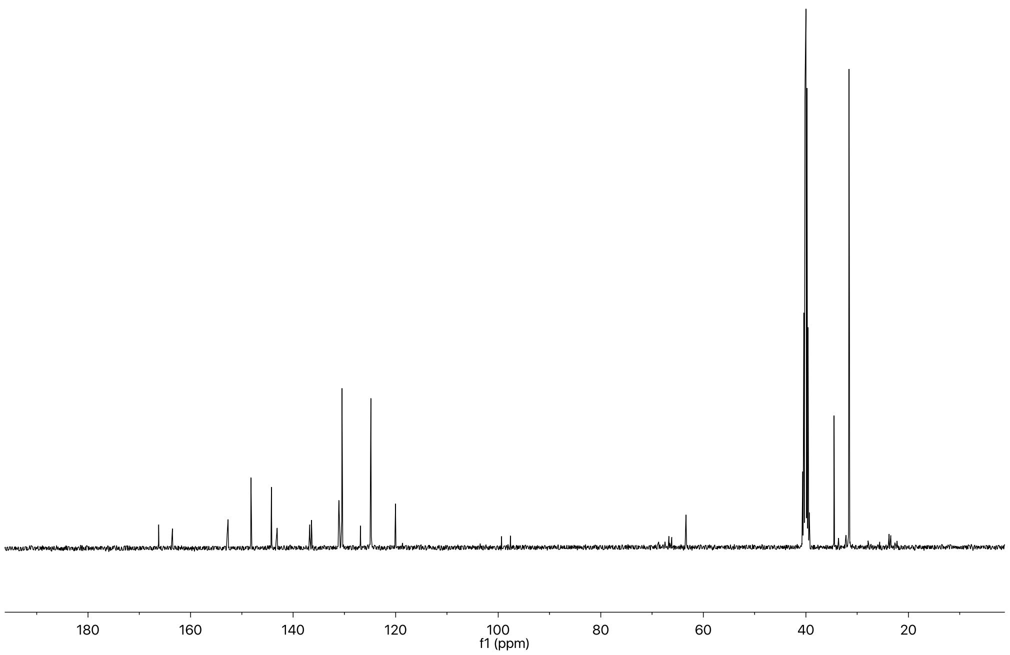

Figure S5 ^{13}C NMR spectrum of **4** (DMSO-d_6, 298 K, 101 MHz).

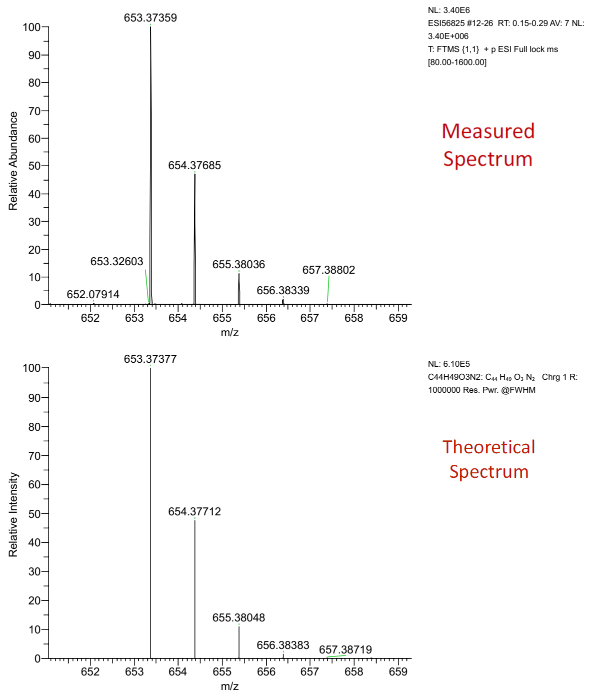

Figure S6 High resolution ESI mass spectrum of **4**.

Terphenyl-stoppered bis-amide azide 5

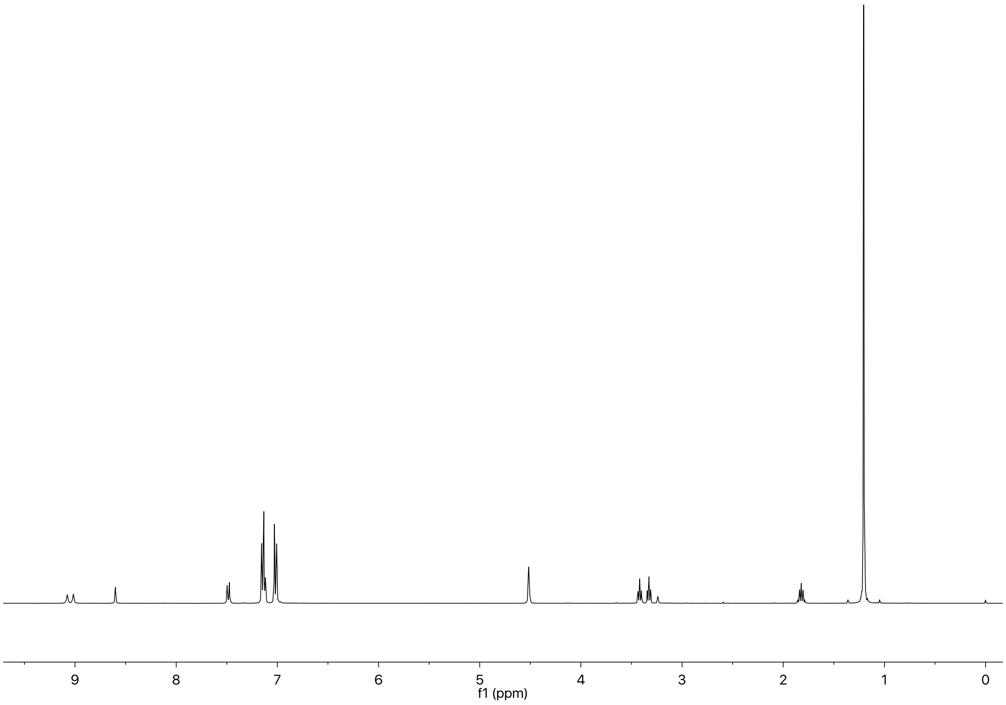

Figure S7 ^{1}H NMR spectrum of **5** (1:1 $CDCl_3$-CD_3OD, 298 K, 400 MHz).

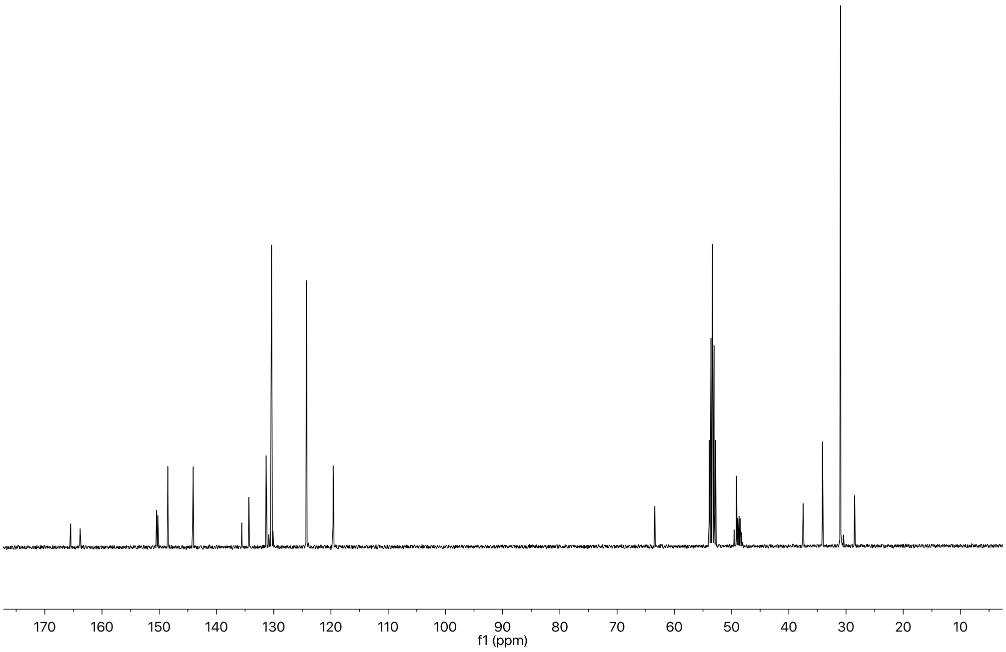

Figure S8 ^{13}C NMR spectrum of **5** (1:1 $CDCl_3$-CD_3OD, 298 K, 101 MHz).

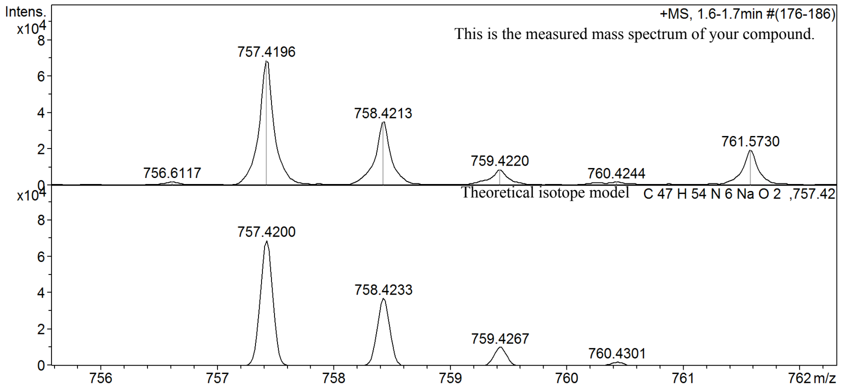

Meas. m/z	#	Formula	m/z	err [ppm]	Mean err [ppm]	rdb	e^- Conf	mSigma
757.4196	1	C 47 H 54 N 6 Na O 2	757.4200	0.6	1.8	23.5	even	16.98

Figure S9 High resolution ESI mass spectrum of **5**.

Terphenyl-stoppered bis-amide pyridinium azide axle precursor 6.Cl

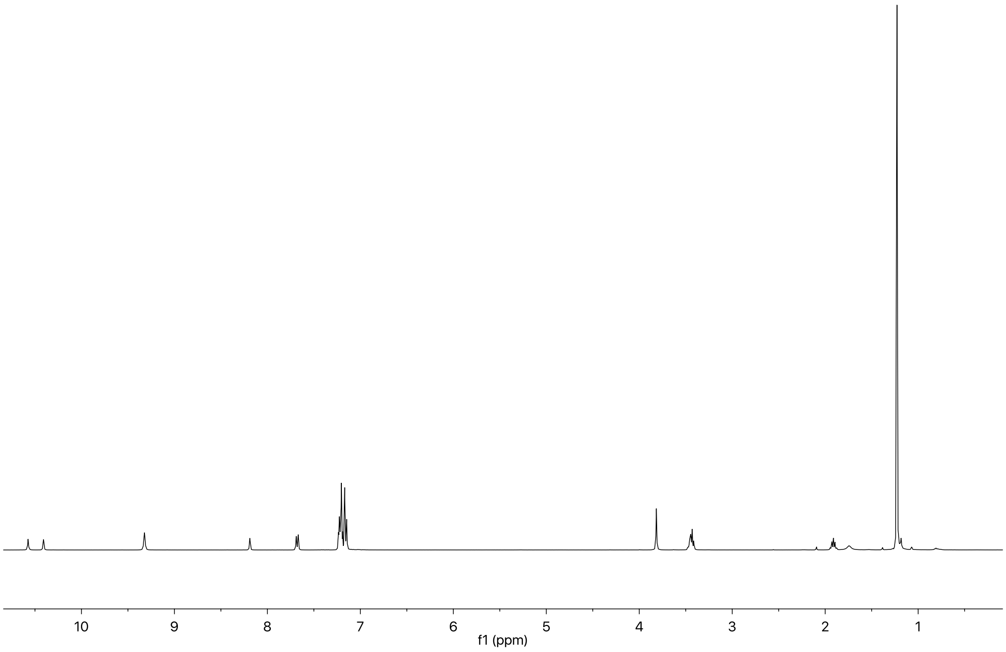

Figure S10 ^{1}H NMR spectrum of **6.Cl** ($CDCl_3$, 298 K, 400 MHz).

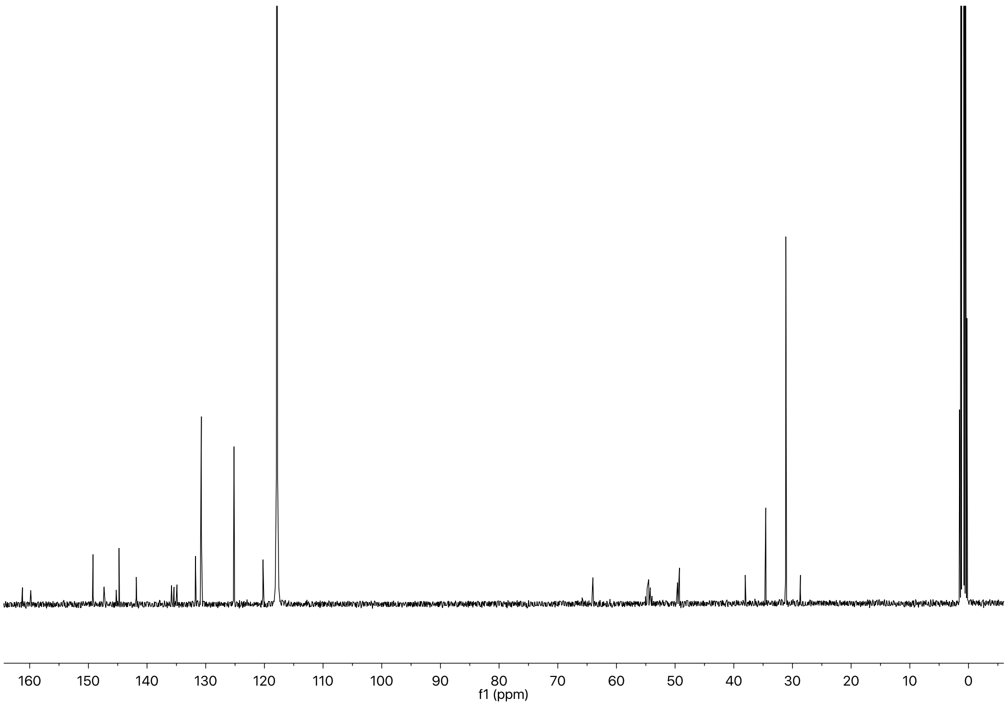

Figure S11 ^{13}C NMR spectrum of **6.Cl** (CD_3CN, 298 K, 101 MHz).

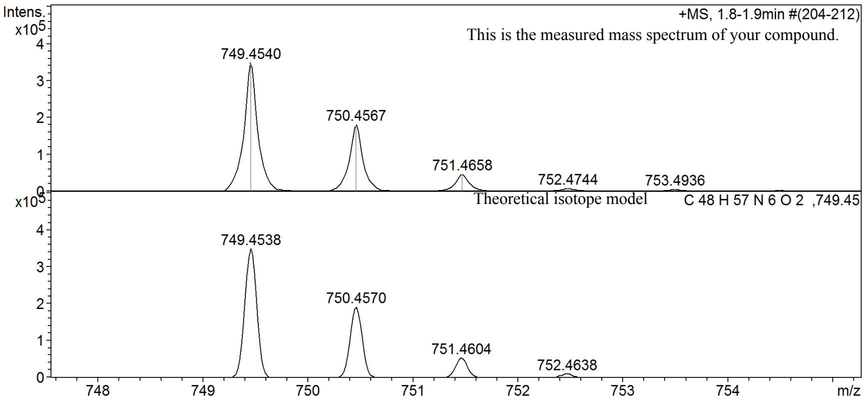

Figure S12 High resolution ESI mass spectrum of **6.Cl**.

Characterisation of rotaxanes 10.PF$_6$ and 11.PF$_6$

Triazole Rotaxane 10.PF$_6$

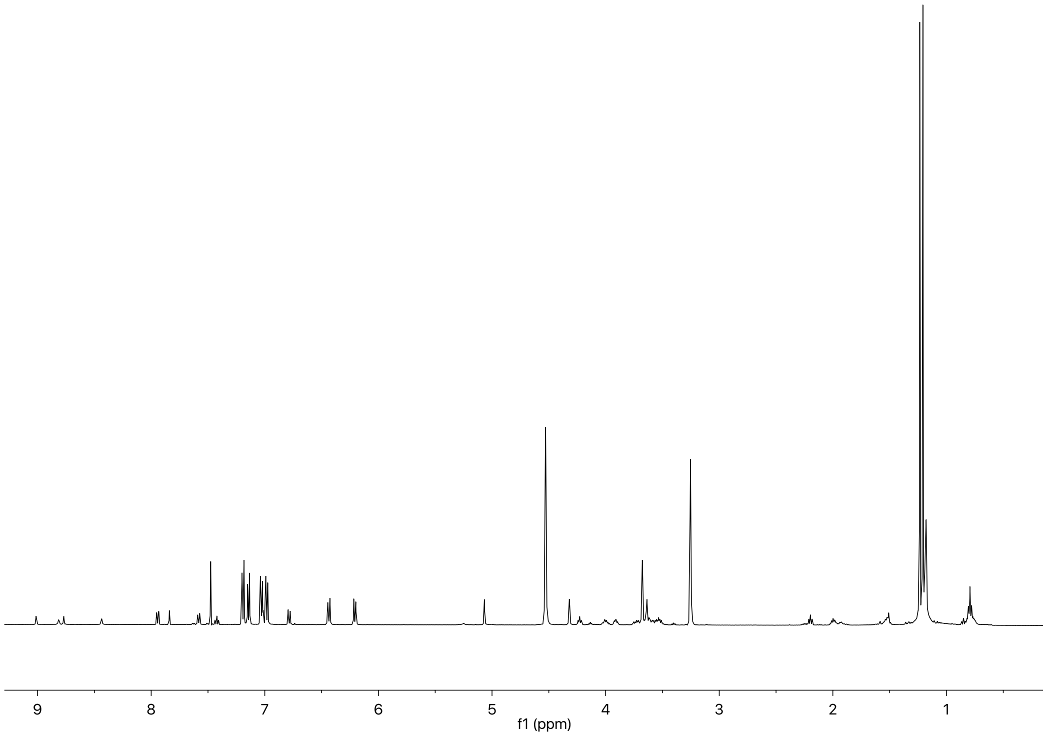

Figure S13 ^{1}H NMR spectrum of rotaxane **10.PF$_6$** (1:1 CDCl$_3$-CD$_3$OD, 298 K, 500 MHz).

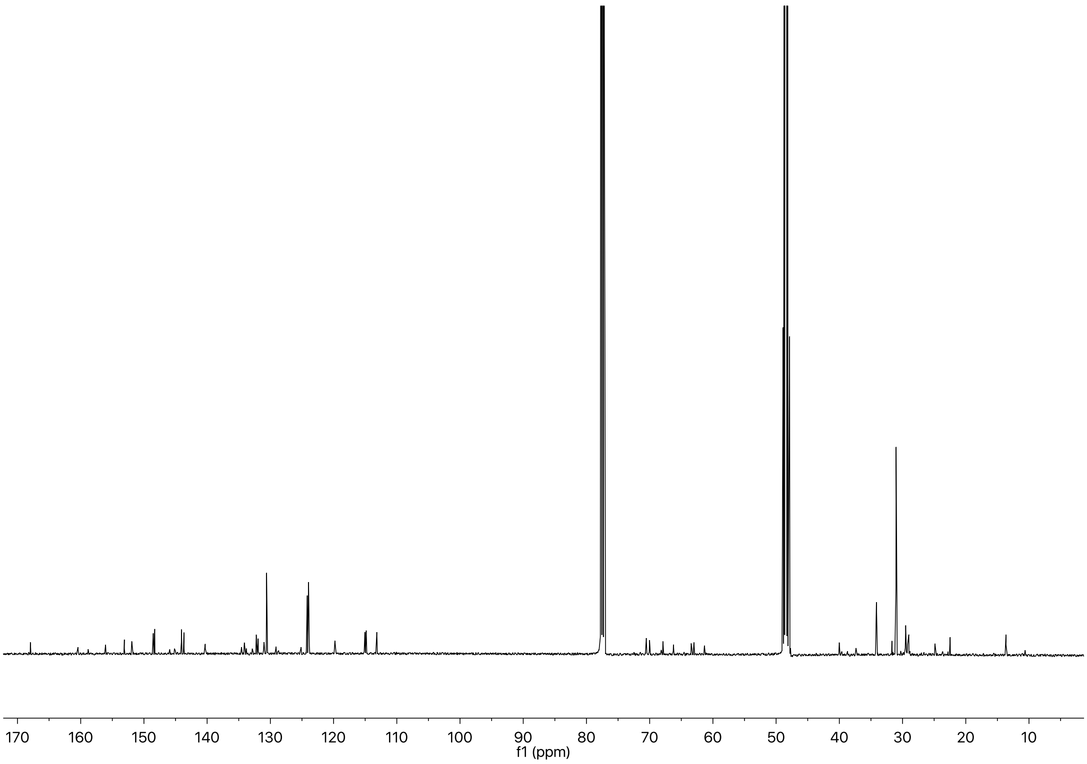

Figure S14 ^{13}C NMR spectrum of rotaxane **10.PF$_6$** (1:1 CDCl$_3$-CD$_3$OD, 298 K, 126 MHz).

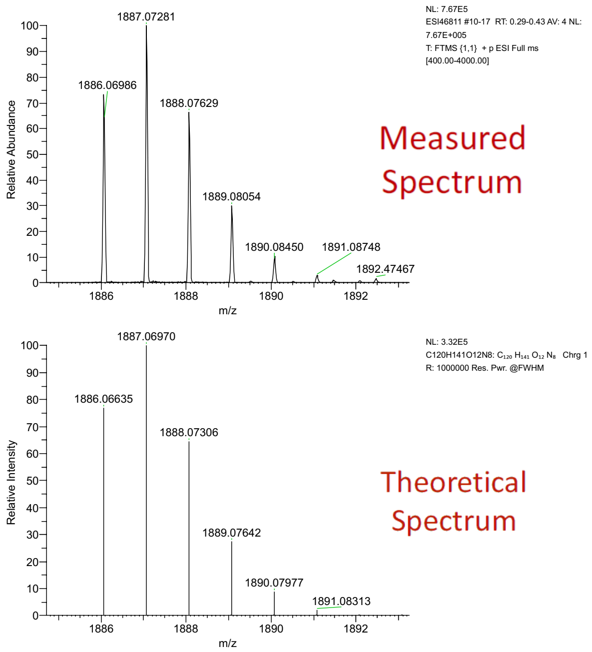

Figure S15 High resolution ESI mass spectrum of rotaxane **10.PF$_6$**.

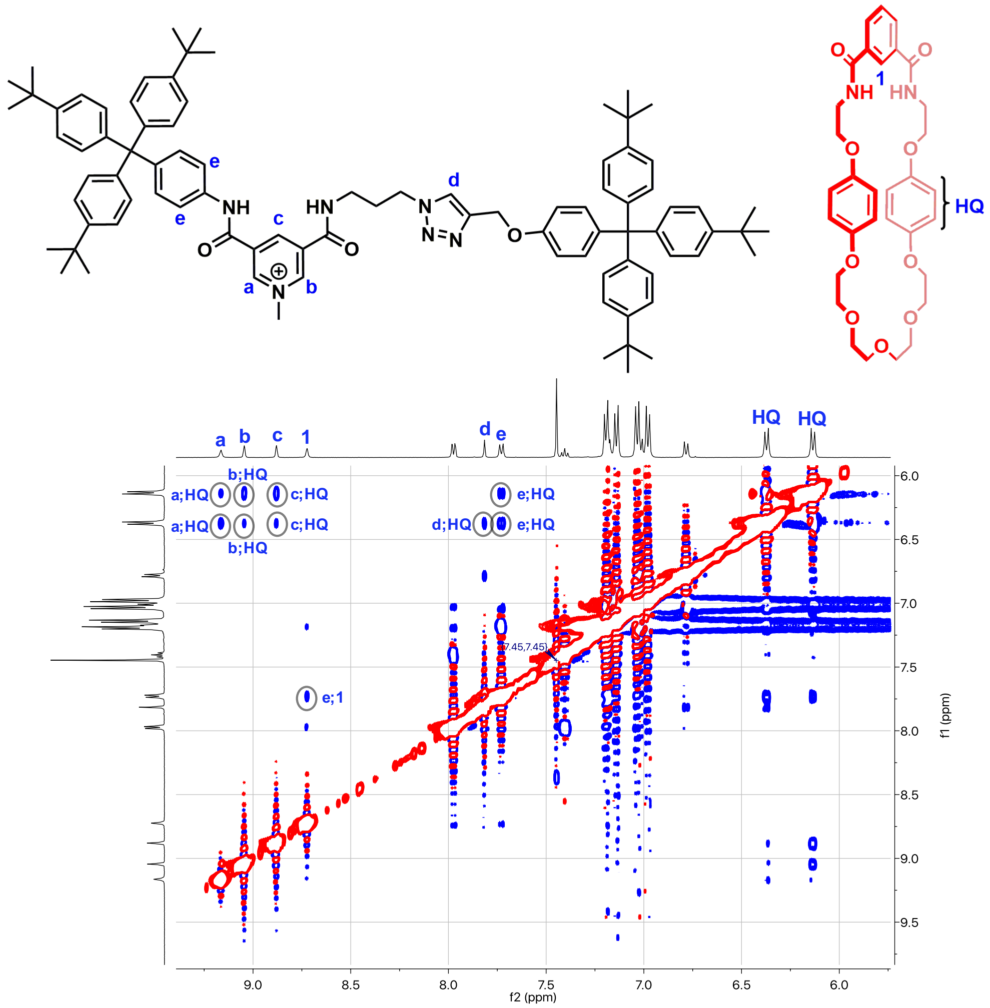

Figure S16 Truncated ^{1}H-^{1}H ROESY NMR spectrum of rotaxane **10.PF$_6$** with 10 through space coupling interactions highlighted with grey circles (1:1 $CDCl_3$-CD_3OD, 298 K, 500 MHz).

Iodotriazole rotaxane 11.PF$_6$

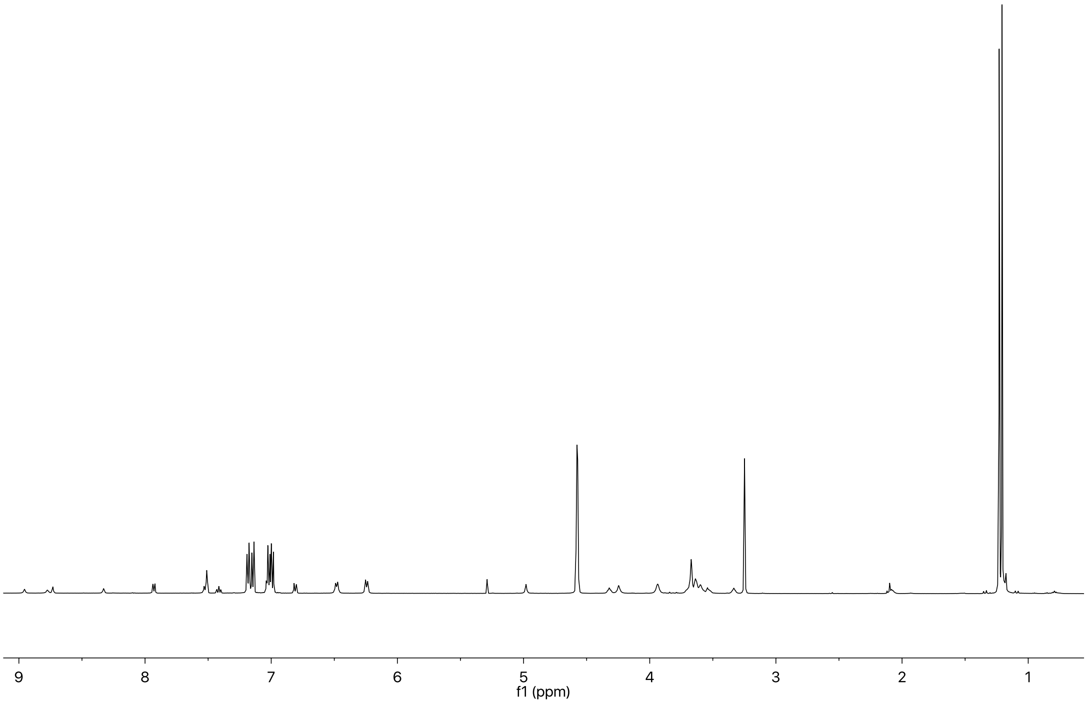

Figure S17 ^{1}H NMR spectrum of rotaxane **11.PF$_6$** (1:1 $CDCl_3$-CD_3OD, 298 K, 500 MHz).

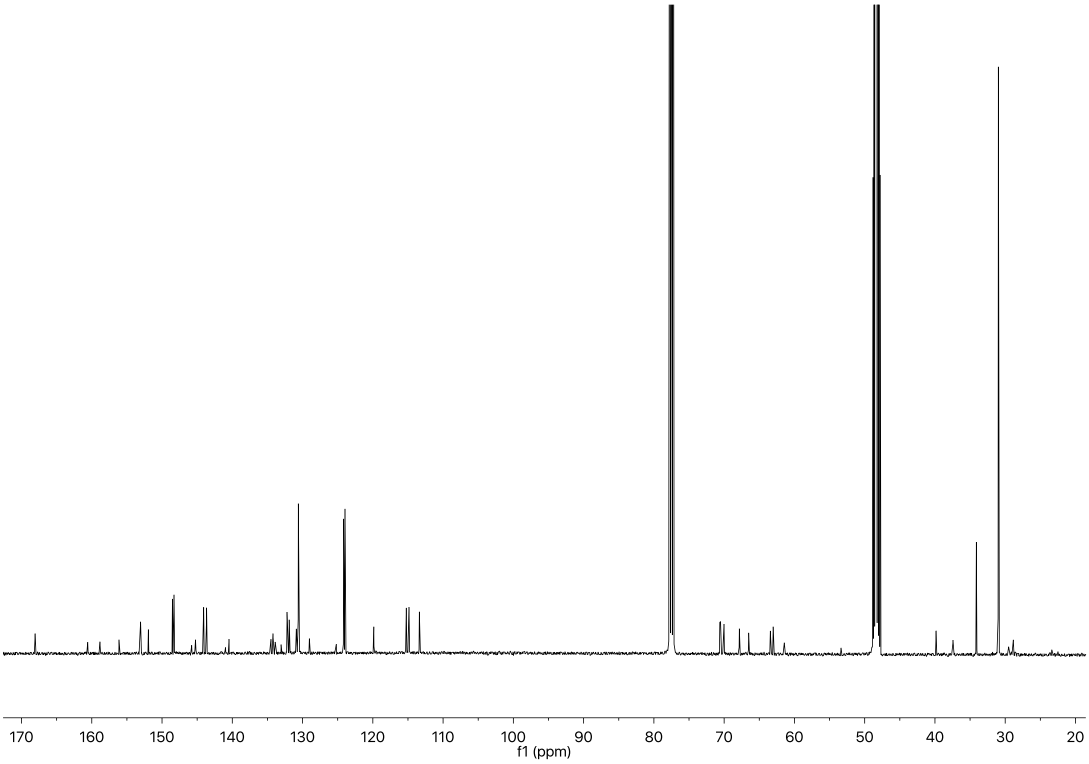

Figure S18 ^{13}C NMR spectrum of rotaxane **11.PF$_6$** (1:1 $CDCl_3$-CD_3OD, 298 K, 126 MHz).

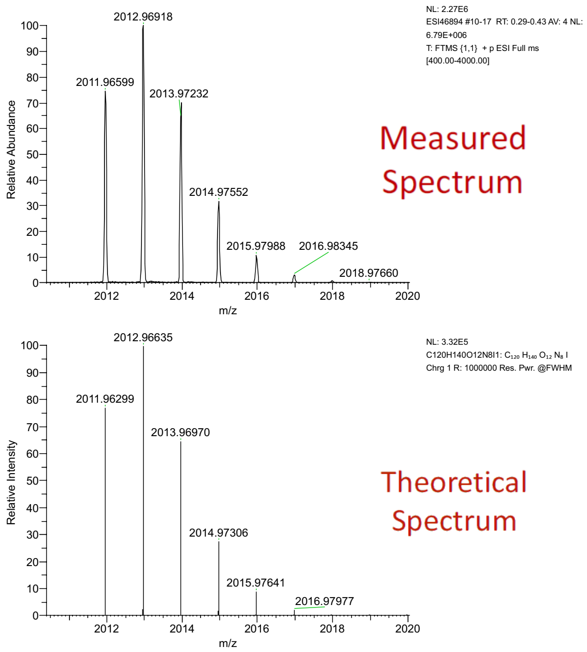

Figure S19 High resolution mass spectrum of rotaxane **11.PF$_6$**.

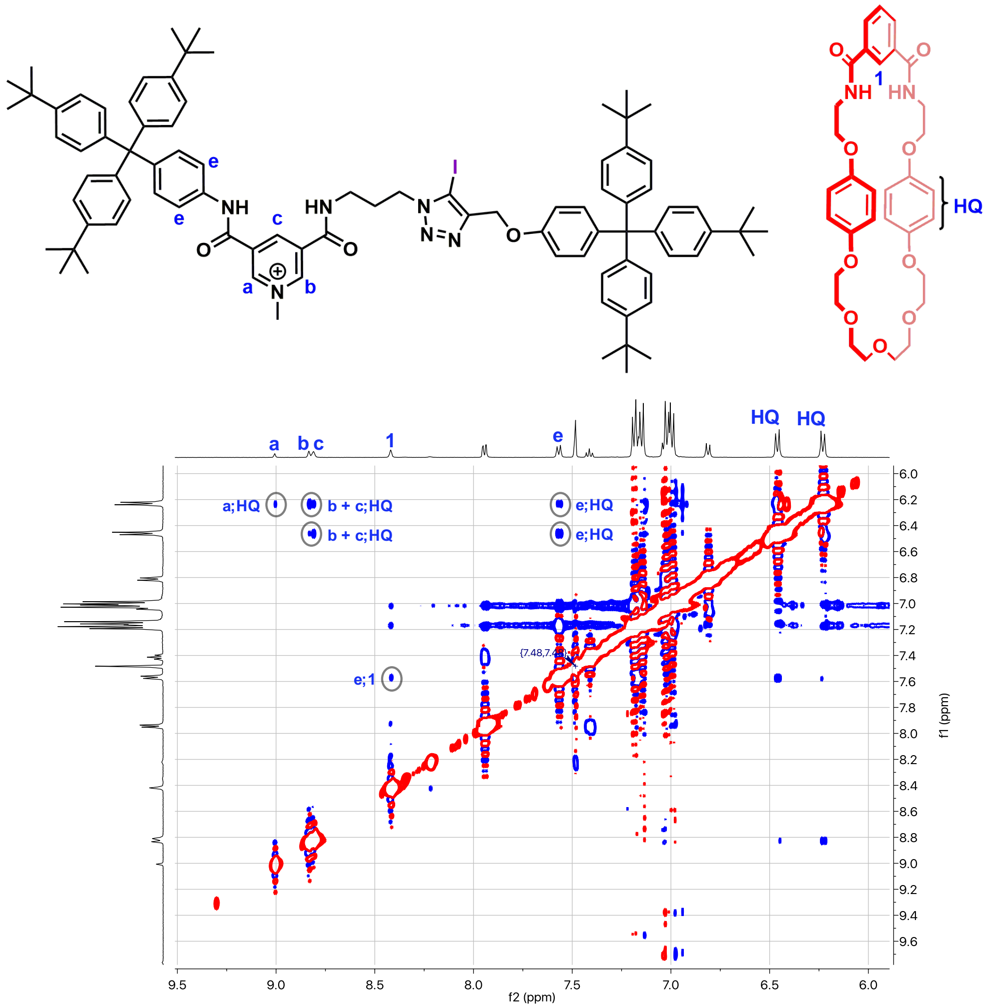

Figure S20 Truncated ^{1}H-^{1}H ROESY NMR spectrum of rotaxane **11.PF$_6$** with 8 through space coupling interactions highlighted with grey circles (1:1 CDCl$_3$-CD$_3$OD, 298 K, 500 MHz).

Characterisation of rotaxanes 12.$(PF_6)_2$ and 13.$(PF_6)_2$

Triazolium Rotaxane 12.$(PF_6)_2$

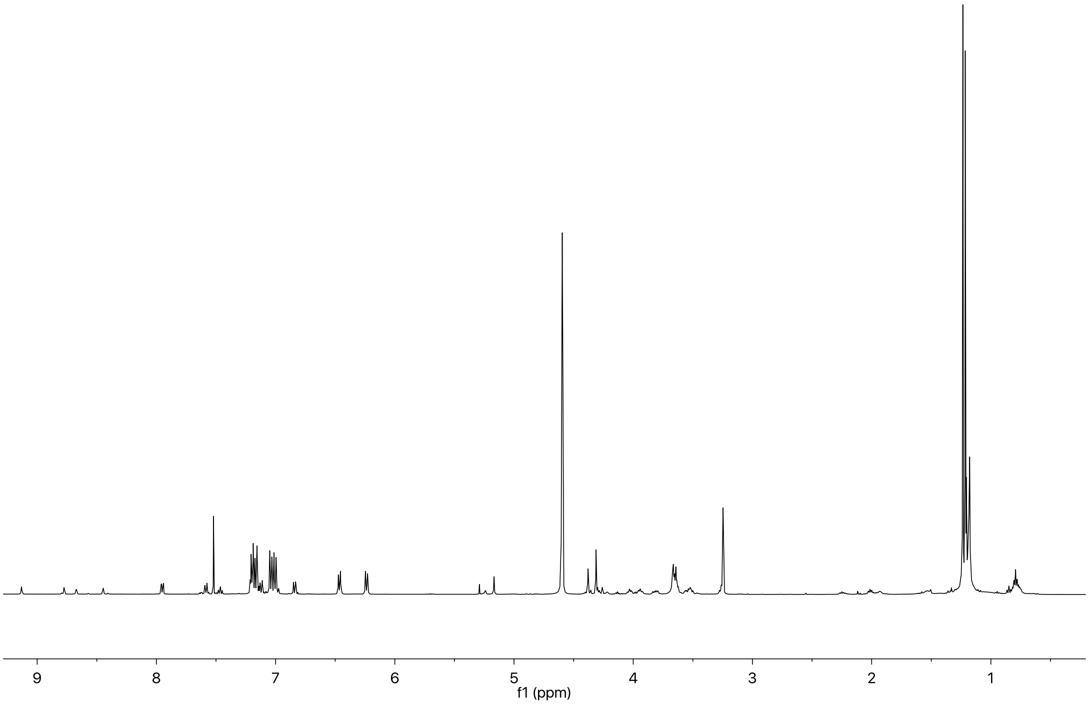

Figure S21 ^1H NMR spectrum of rotaxane **12.$(PF_6)_2$** (1:1 $CDCl_3$-CD_3OD, 298 K, 500 MHz).

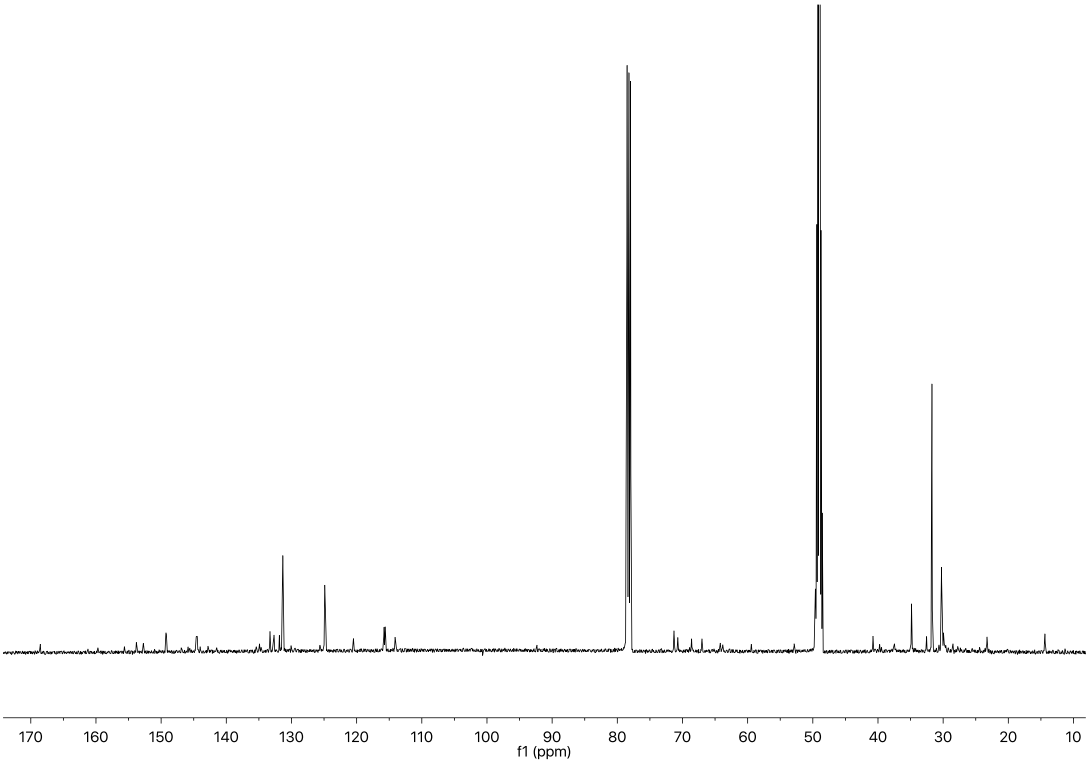

Figure S22 ^{13}C NMR spectrum of rotaxane **12.$(PF_6)_2$** (1:1 $CDCl_3$-CD_3OD, 298 K, 126 MHz).

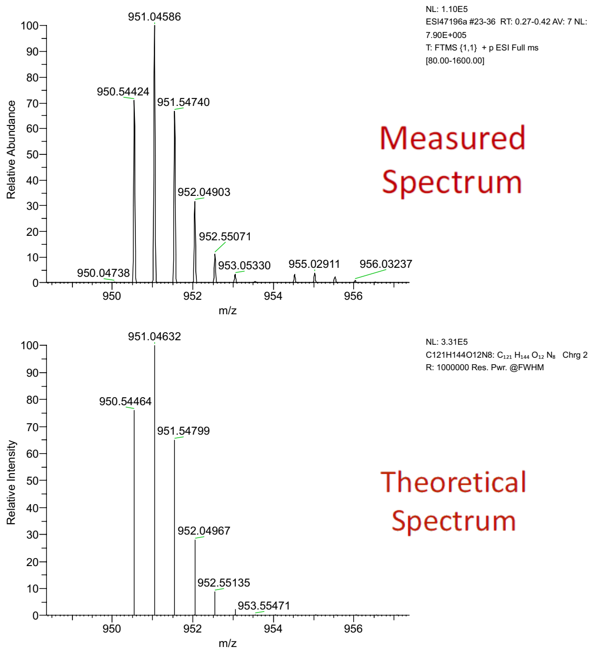

Figure S23 High resolution mass spectrum of rotaxane **12.(PF$_6$)$_2$**.

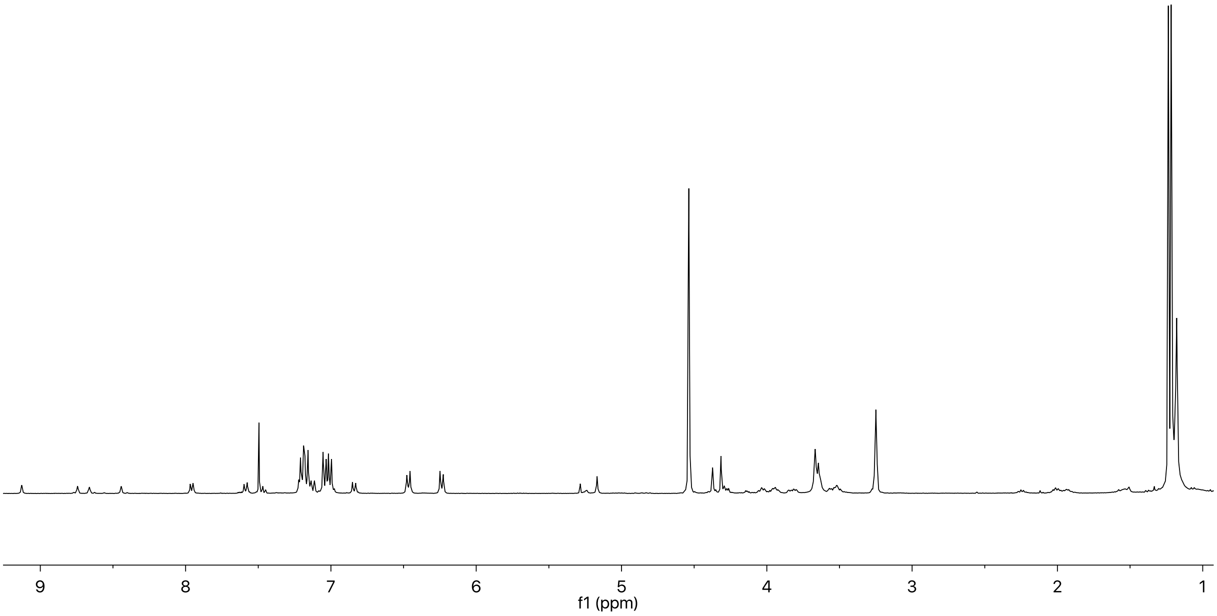

Figure S24 ^{1}H NMR spectrum of rotaxane **13.(PF$_6$)$_2$** (1:1 CDCl$_3$-CD$_3$OD, 298 K, 500 MHz).

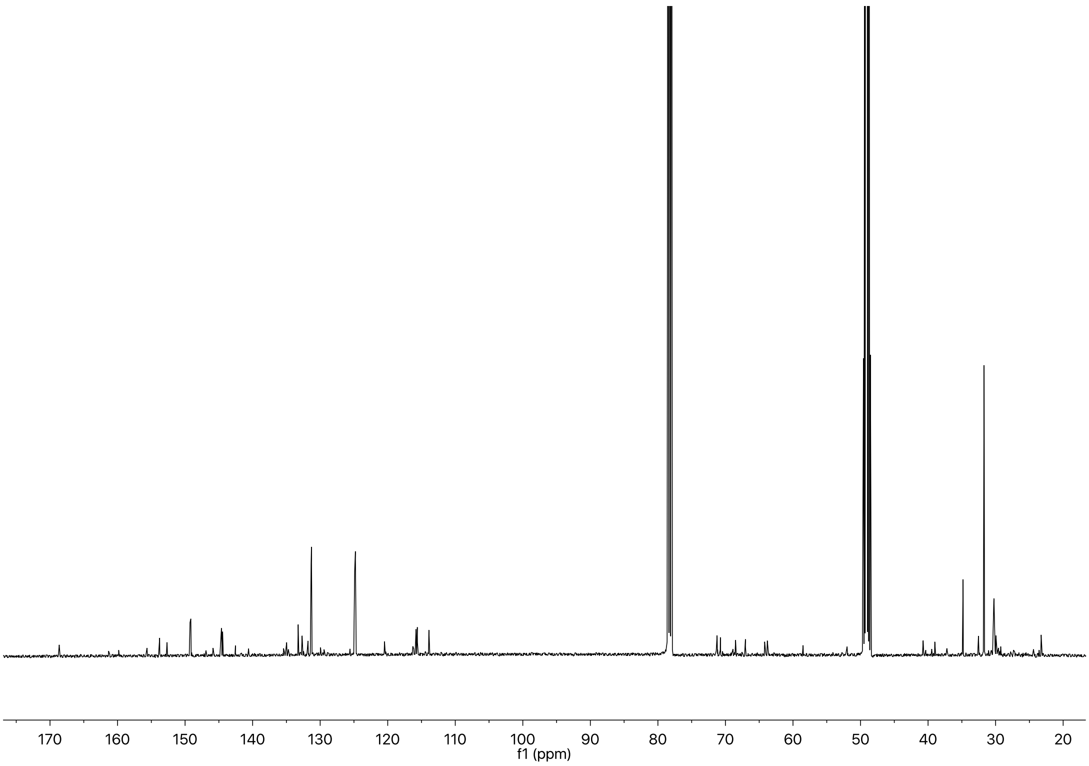

Figure S25 ^{13}C NMR spectrum of rotaxane **13.(PF$_6$)$_2$** (1:1 $CDCl_3$-CD_3OD, 298 K, 126 MHz).

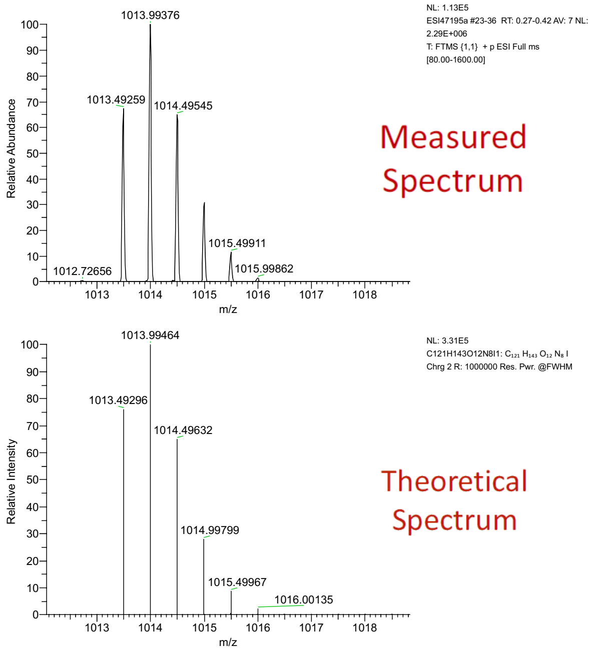

Figure S26 High resolution mass spectrum of rotaxane **13.(PF$_6$)$_2$**.

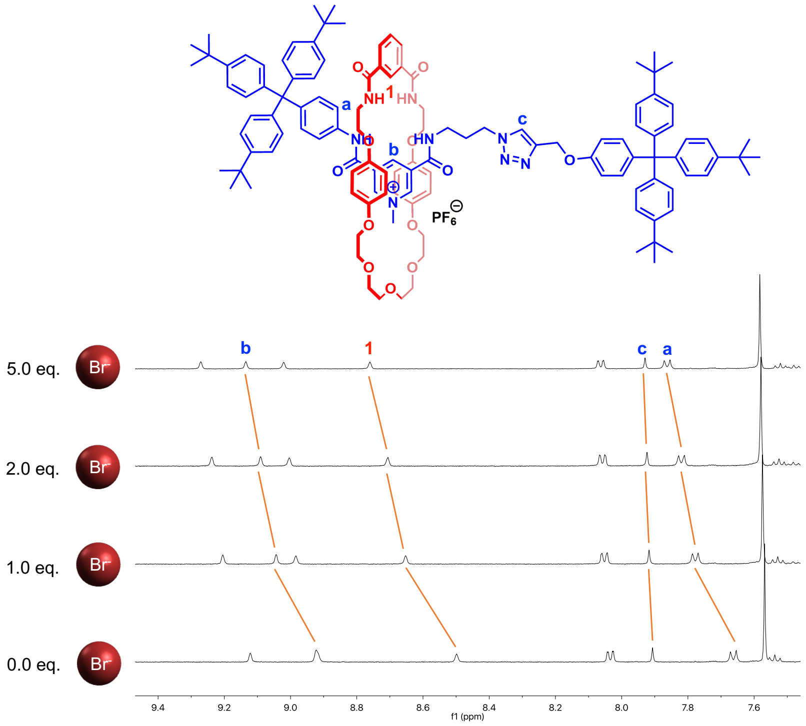

Figure S27 Changes in the ^{1}H NMR spectrum of HB rotaxane **10.PF$_6$** on addition of increasing equivalents of TBABr (45:45:10 CDCl$_3$-CD$_3$OD-D$_2$O, 500 MHz, 298 K).

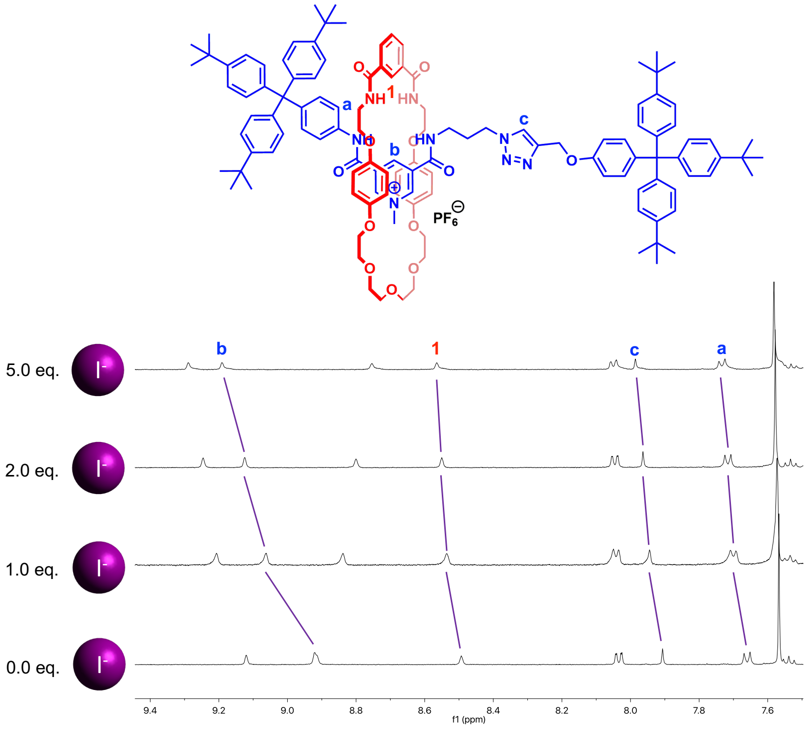

Figure S28 Changes in the ^{1}H NMR spectrum of HB rotaxane **10.PF$_6$** on addition of increasing equivalents of TBAI (45:45:10 CDCl$_3$-CD$_3$OD-D$_2$O, 500 MHz, 298 K).

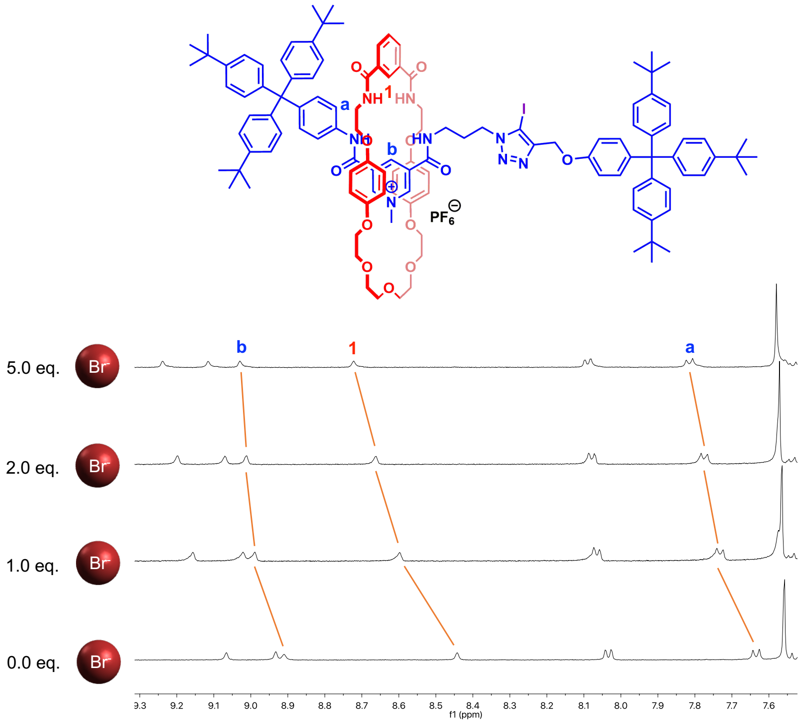

Figure S29 Changes in the ^{1}H NMR spectrum of XB rotaxane **$11.PF_6$** on addition of increasing equivalents of TBABr (45:45:10 $CDCl_3$-CD_3OD-D_2O, 500 MHz, 298 K).

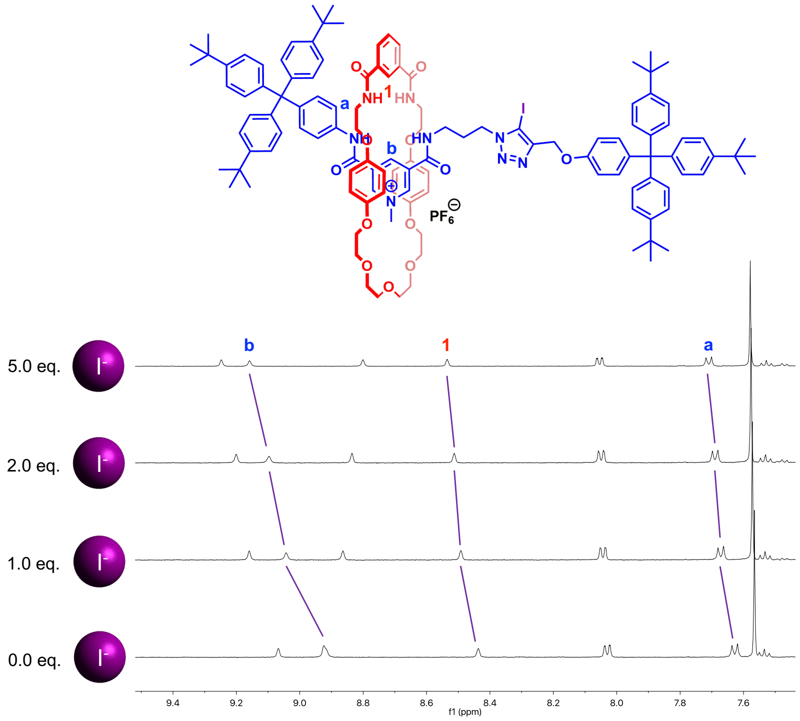

Figure S30 Changes in the ^{1}H NMR spectrum of XB rotaxane **$11.PF_6$** on addition of increasing equivalents of TBAI (45:45:10 $CDCl_3$-CD_3OD-D_2O, 500 MHz, 298 K).

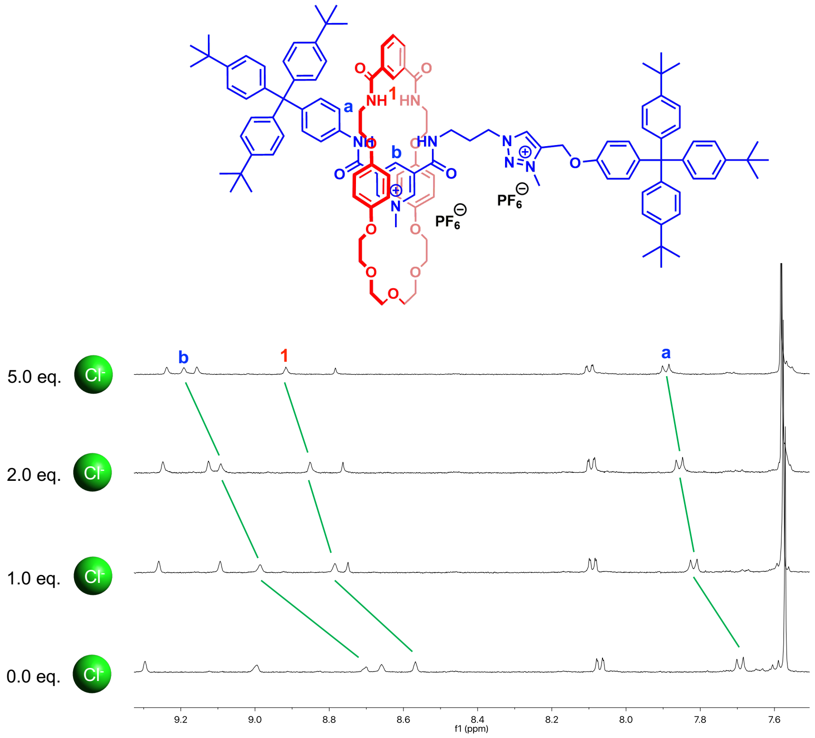

Figure S31 Changes in the ^{1}H NMR spectrum of HB rotaxane **12.(PF$_6$)$_2$** on addition of increasing equivalents of TBACl (45:45:10 $CDCl_3$-CD_3OD-D_2O, 500 MHz, 298 K).

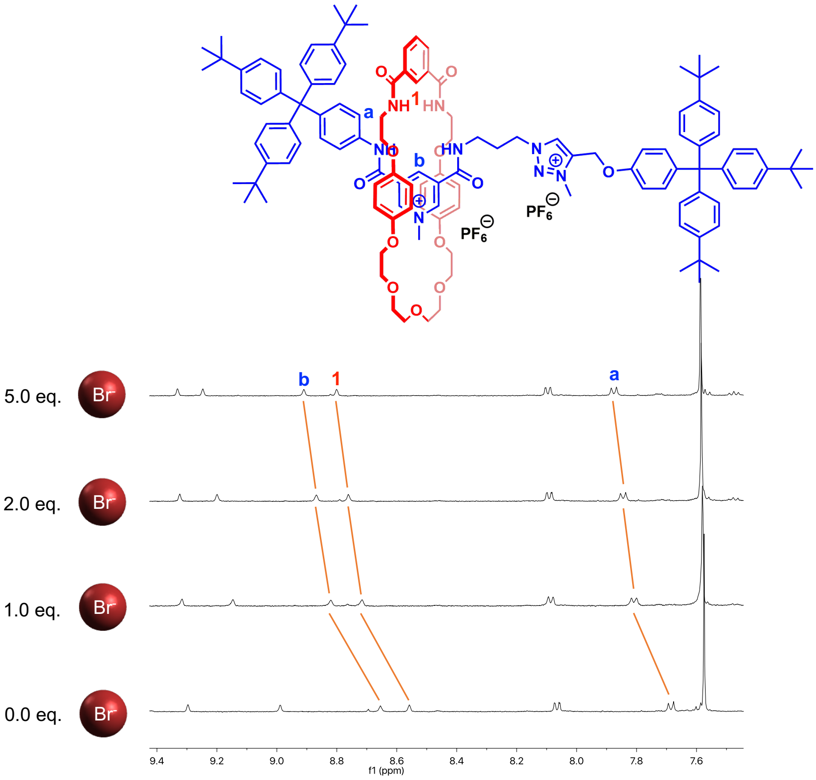

Figure S32 Changes in the ^{1}H NMR spectrum of HB rotaxane **12.(PF$_6$)$_2$** on addition of increasing equivalents of TBABr (45:45:10 $CDCl_3$-CD_3OD-D_2O, 500 MHz, 298 K).

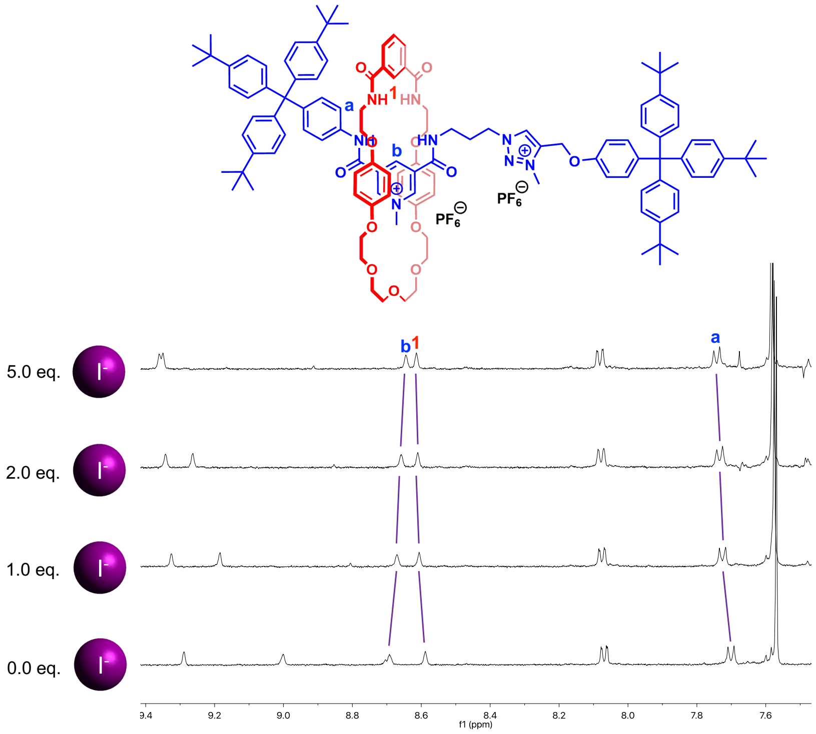

Figure S33 Changes in the ^{1}H NMR spectrum of HB rotaxane **12.(PF$_6$)$_2$** on addition of increasing equivalents of TBAI (45:45:10 $CDCl_3$-CD_3OD-D_2O, 500 MHz, 298 K).

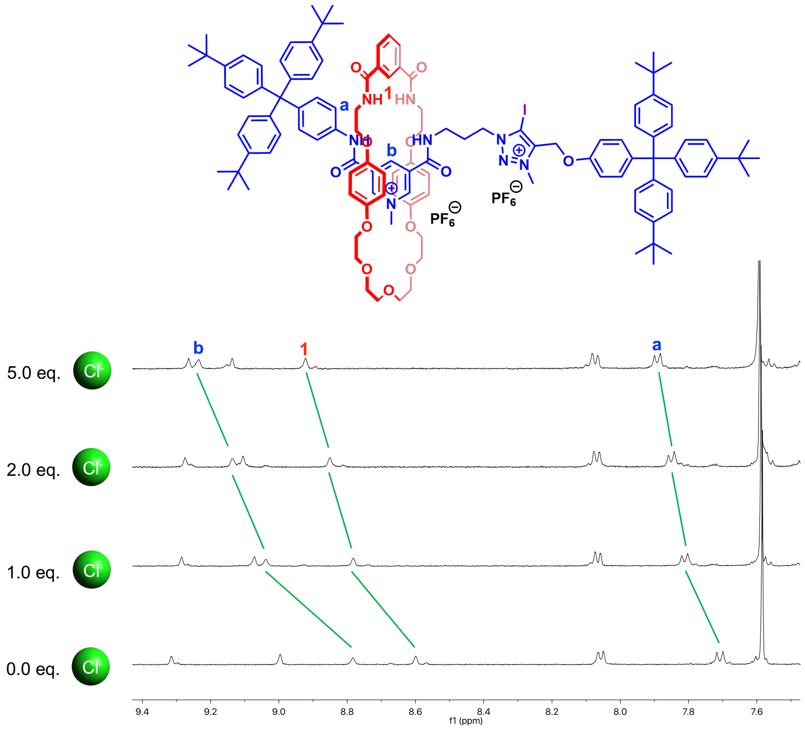

Figure S34 Changes in the ^{1}H NMR spectrum of XB rotaxane **13.(PF$_6$)$_2$** on addition of increasing equivalents of TBACl (45:45:10 $CDCl_3$-CD_3OD-D_2O, 500 MHz, 298 K).

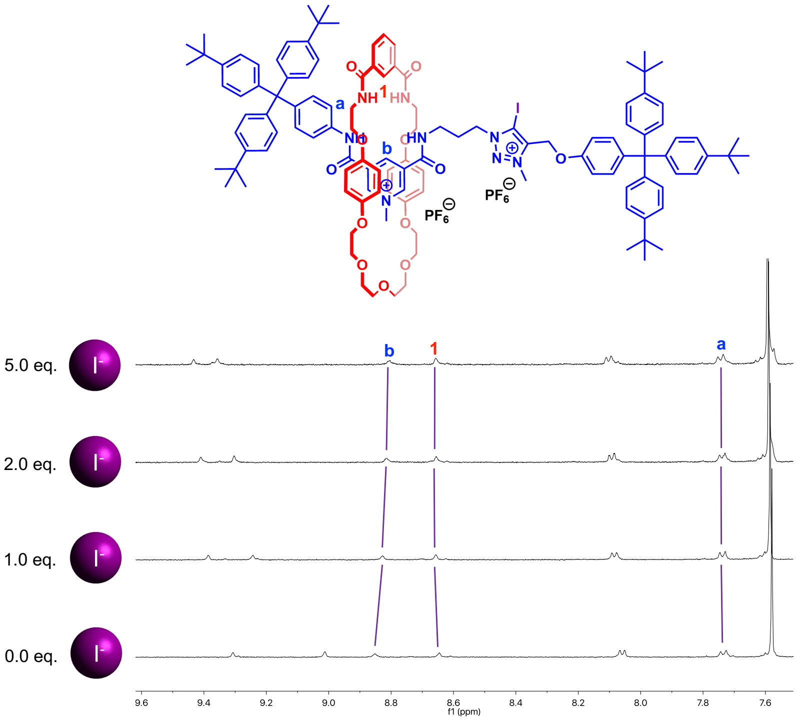

Figure S35 Changes in the ^{1}H NMR spectrum of XB rotaxane **13.(PF$_6$)$_2$** on addition of increasing equivalents of TBAI (45:45:10 $CDCl_3$-CD_3OD-D_2O, 500 MHz, 298 K).

References

S1 B.-Y. Lee, S. R. Park, H. B. Jeon and K. S. Kim, *Tetrahedron Lett.*, 2006, **47**, 5105–5109.

S2 M. J. Hynes, *J. Chem. Soc. Dalton Trans.*, 1993, 311–312.